

Article

Allometric Scaling and Resource Limitations Model of Tree Heights: Part 3. Model Optimization and Testing over Continental China

Xiliang Ni ^{1,2,†}, Taejin Park ^{2,*†}, Sungho Choi ², Yuli Shi ^{2,3}, Chunxiang Cao ¹, Xuejun Wang ⁴, Michael A. Lefsky ⁵, Marc Simard ⁶ and Ranga B. Myneni ²

¹ State Key Laboratory of Remote Sensing Science, Institute of Remote Sensing and Digital Earth, Chinese Academy of Sciences, Beijing 100101, China; E-Mails: nixl@irsa.ac.cn (X.N.); cao413@irsa.ac.cn (C.C.)

² Department of Earth and Environment, Boston University, 675 Commonwealth Avenue, Boston, MA 02215, USA; Emails: schoi@bu.edu (S.C.); ylshi.nuist@gmail.com (Y.S.); ranga.myneni@gmail.com (R.B.M.)

³ School of Remote Sensing, Nanjing University of Information Science and Technology, Nanjing 210044, China

⁴ Survey Planning and Design Institute, State Forest Administration of China, Beijing 100714, China; E-Mail: wangxuejun320@126.com

⁵ Center for Ecological Analysis of Lidar, Natural Resource Ecology Laboratory, Colorado State University, Fort Collins, CO 80523, USA; E-Mail: lefsky@cnr.colostate.edu

⁶ Jet Propulsion Laboratory, California Institute of Technology, Pasadena, CA 91109, USA; E-Mail: marc.simard@jpl.nasa.gov

† These authors contributed equally to this work.

* Author to whom correspondence should be addressed; E-Mail: partj@bu.edu; Tel.: +1-617-893-1988; Fax: +1-617-353-8399.

Received: 7 February 2014; in revised form: 3 April 2014 / Accepted: 15 April 2014 /

Published: 25 April 2014

Abstract: The ultimate goal of our multi-article series is to demonstrate the Allometric Scaling and Resource Limitation (ASRL) approach for mapping tree heights and biomass. This third article tests the feasibility of the optimized ASRL model over China at both site (14 meteorological stations) and continental scales. Tree heights from the Geoscience Laser Altimeter System (GLAS) waveform data are used for the model optimizations. Three selected ASRL parameters (area of single leaf, α ; exponent for canopy radius, η ; and

root absorption efficiency, γ) are iteratively adjusted to minimize differences between the references and predicted tree heights. Key climatic variables (e.g., temperature, precipitation, and solar radiation) are needed for the model simulations. We also exploit the independent GLAS and *in situ* tree heights to examine the model performance. The predicted tree heights at the site scale are evaluated against the GLAS tree heights using a two-fold cross validation (RMSE = 1.72 m; $R^2 = 0.97$) and bootstrapping (RMSE = 4.39 m; $R^2 = 0.81$). The modeled tree heights at the continental scale (1 km spatial resolution) are compared to both GLAS (RMSE = 6.63 m; $R^2 = 0.63$) and *in situ* (RMSE = 6.70 m; $R^2 = 0.52$) measurements. Further, inter-comparisons against the existing satellite-based forest height maps have resulted in a moderate degree of agreements. Our results show that the optimized ASRL model is capable of satisfactorily retrieving tree heights over continental China at both scales. Subsequent studies will focus on the estimation of woody biomass after alleviating the discussed limitations.

Keywords: tree height; allometric scaling law; resource limitation; model optimization; geoscience laser altimeter system (GLAS); national forest inventory (NFI)

1. Introduction

Forest structural attributes are crucial indicators for demonstrating forest ecosystem services [1]. In particular, the spatio-temporal patterns of forest height (potentially biomass) provide regional or global contexts of terrestrial carbon fluxes and storages [2–4]. Due to the broad geographical extent, large spatial variability and the limited accessibility for field inventories, mapping forest heights at a larger scale generally relies on three-dimensional (3D) remote sensing techniques such as light or radio detection and ranging (lidar or radar) systems [5–8]. For instance, the Geoscience Laser Altimeter System (GLAS) is the first spaceborne lidar instrument providing reasonable vertical profiles of forests with global coverage [9]. However, because of its intrinsic discrete sampling scheme, GLAS needs additional extrapolation procedures to produce wall-to-wall forest height maps. Recent studies have used several statistical models based on valid relationships between forest heights and geospatial predictors, which have produced spatially continuous forest height maps depicting the spatial variation in vertical forest structures [5–8,10,11]. Nevertheless, their extrapolation approaches are likely to depend on input data quality and quantity, and often neglect the physical/physiological mechanisms governing tree growth.

For better mechanistic understanding in mapping forest heights, Kempes *et al.* [12] presented the Allometric Scaling Resource Limitation (ASRL) model composed of two conceptual schemes: (a) allometric scaling laws may provide a valid tree geometry [13,14] and (b) potential tree growth is constrained by local resources (e.g., water, temperature, sunlight, and wind) [15]. However, the ASRL model with universal allometric coefficients and scaling exponents shows less predictive power when applied to diverse eco-climatic regimes and forest types of varying age classes [16,17]. Thus, a synergistic combination of physical/physiological mechanism (*i.e.*, ASRL approach) and 3D remote sensing techniques (*i.e.*, GLAS) has recently been explored using parametric optimizations [16,17].

The first [16] in a multi-article series has provided a thorough description of the optimized ASRL model. The GLAS altimetry is implemented to iteratively adjust three selected ASRL parameters (area of single leaf, α , exponent for canopy radius, η , and root absorption efficiency, γ). This parametric optimization minimizes disparities between the reference and modeled tree heights. The optimized ASRL model results in a contiguous map of the maximum forest heights over the continental USA (CONUS) at the 1 km spatial resolution, and shows a moderate predictive power with a root mean square error (RMSE) of 3.31 m and a coefficient of determination (R^2) of 0.59 (from a two-fold cross validation). This showed the feasibility of the optimized ASRL model for large-scale mapping. The second study [17] in this series examined the above approach at a finer spatial scale, *i.e.*, FLUXNET sites, where more accurate input information is available. This site-scale test shows a satisfactory performance of the optimized ASRL model through the two-fold cross validation ($R^2 = 0.85$; RMSE = 1.81 m) and bootstrapping evaluation ($R^2 = 0.66$; RMSE = 2.60 m).

Based on the experiments over the CONUS in the previous two articles, our scientific question aroused here is if the optimized ASRL model is applicable to other forest ecosystems, *e.g.*, over the continental China (CONNA). The geographical extents and the diversity in climate, topography, forest types of the CONNA are comparable to those of the CONUS. Therefore, this third study aims to test the optimized ASRL model over the CONNA at both site and continental scales. In this study, we produced the modeled heights for Chinese forests using the same manner used in previous articles [16,17]. The evaluations were made against field-measured and GLAS-derived tree heights. In addition, the spatially continuous field of maximum tree heights (1 km resolution) over the CONNA was compared against the existing forest height maps from Lefsky [7] and Simard *et al.* [8]. This study briefly introduced the optimized ASRL model along with input variables and key allometric scaling parameters. Since we are examining the applicability of the model across different forest ecosystems, our discussions focus more on the final outcomes over the CONNA rather than the initial predictions or the optimization processes whose details are given in previous articles [16,17].

2. Material

2.1. Input Data for the ASRL Model

2.1.1. Climate Data

Input climatic variables for the ASRL model include precipitation, temperature, relative humidity, wind speed, and incoming solar radiation, which determine the available and evaporative flow rates. The ASRL model quantifies resource limitations on tree's growth using these flow rates [12]. This study obtained two types (weather station-based and gridded data) of climate datasets over the CONNA (Table 1).

First, weather station-based climatic variables were used for the site-scale ASRL simulations. The China Meteorological Data Sharing Service System (CMDSSS) provides the annual meteorological records observed from 754 weather stations [18] (Figure S1 of Supplementary Information). This study implemented such observations spanning over 50 years (1951–2007), comprised of annual total precipitation, average temperature, relative humidity, wind speed, and solar radiation time. We further

converted the observed solar radiation time into the incoming solar radiation rate, as needed for the model predictions, using a statistical method suggested by Liao *et al.* [19].

Second, gridded climate datasets (1 km resolution) were exploited in the continental-scale ASRL model simulations. The WorldClim [20] produces long-term (1950–2000) climate maps based on the thin-plate smoothing spline algorithm [21]. As annual total precipitation and average temperature were only available input climate data from the WorldClim, we interpolated other climatic variables from the CMDSSS using ordinary kriging [22] to generate the gridded maps of annual average relative humidity, wind speed, and solar radiation. Uncertainties related to this interpolation process are discussed in Section 4.3.

2.1.2. Ancillary Data

Simulation and optimization procedures of the ASRL model also require other ancillary datasets including digital elevation model (DEM), leaf area index (LAI), land cover (LC), and percent tree cover (Table 1). The DEM and LAI were input ASRL variables to calculate the potential evaporative flow rate of trees, while LC and percent tree cover were used to identify forested lands over the CONNA. In this study, we used the Advanced Spaceborne Thermal Emission and Reflection Radiometer (ASTER) Global DEM (GDEM V2, 30 m grid) [23]. The approximate growing season (June to September) averaged LAI data from 2003 to 2006 were obtained from a refined version of the Moderate Resolution Imaging Spectroradiometer (MODIS) LAI product (1 km grids) [24]. The MODIS global LC (MCD12Q1, 500 m grid) [25] and Vegetation Continuous Field (VCF; MOD44B, 250 m grid) [26] for the year 2005 accounted for the rest of ancillary datasets. To standardize the spatial resolutions, finer gridded ancillary data were resampled into the 1 km resolution using the majority principle technique for categorical values and the cubic convolution method for numerical values [27]. We took into account three forest types (evergreen, deciduous, and mixed forests) aggregated from the five International Geosphere-Biosphere Programme (IGBP) forest classes, and forested lands were defined by a percent tree cover ($\geq 50\%$) based on the VCF product (Figure 1). The above-described ancillary datasets were used in the ASRL model simulations at both site and continental scales.

2.1.3. Eco-Climatic Zone

For the computationally practical model optimizations (see Section 3.1), we separately defined the eco-climatic zones over the CONNA, accounting for three forest types, annual total precipitation (30 mm intervals) and annual average temperature (2 °C intervals). This classification resulted in 537 zones at the site scale and 5805 zones at the continental scale. This zonal information was used as the basic element (unit or level) in the model optimization and evaluation process.

2.2. Tree Height Measurements

2.2.1. GLAS-Derived Tree Heights

The GLAS-derived tree heights over the CONNA were used to optimize the ASRL parameters and to assess the model's performance. In this study, we obtained the latest release of GLAS laser altimetry

data (Release-33) from the National Snow and Ice Data Center. Amongst various altimetry products of the Release-33, the level-2 data (*i.e.*, GLA14) were selected for the maximum tree height retrieval. The GLA14 provides metrics for land surface elevation along with the geo-location of laser footprints and the waveform parameters, such as signal beginning and echo energy peaks [28]. We exploited the GLAS data recorded from May to October (2003–2006) because this seasonal period represents the best approximate of forests' leaf-on condition. The defoliation of deciduous forests may generate underestimations in the GLAS-derived maximum tree heights. As it is impractical to estimate the ellipsoidal shapes and sizes for each footprint [29], this study assumed that all the GLAS footprints are likely to have a circular shape with a diameter of 70 m [30].

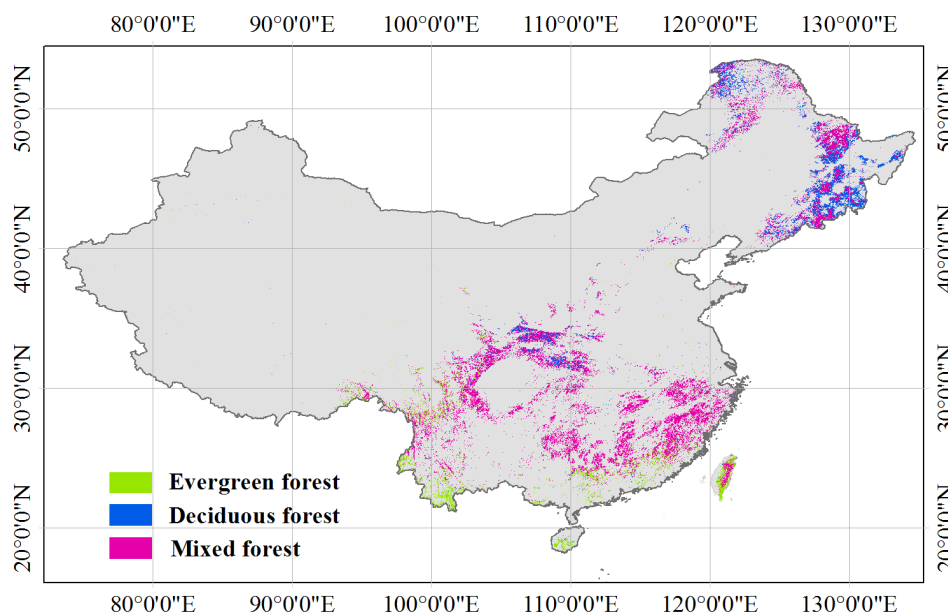
Table 1. Climatic and ancillary datasets prepared for the Allometric Scaling and Resource Limitation (ASRL) model.

| Types | Input Variable | Unit | Spatial Resolution | Temporal Range | Source |
|-------------------|-----------------------------------|------------------|-----------------------|-----------------------------|-------------------------------|
| Climate dataset | Annual Average Relative Humidity | % | Weather station-based | 1951–2007 | CMDSSS [18] |
| | Annual Average Wind Speed | m/s | | | |
| | Annual Incoming Solar Radiation * | W/m ² | | | |
| | Annual Total Precipitation | mm | | | |
| | Annual Average Temperature | °C | | | |
| | Annual Total Precipitation | mm | | | |
| Ancillary dataset | Annual Average Temperature | °C | 1 km | 1950–2000 | WorldClim [20] |
| | DEM | m | 30 m | 2011 | ASTER GDEM V2 [23] |
| | Growing Season Averaged LAI | N/A | 1 km | 2003–2006 June–September | Post-processed MODIS LAI [24] |
| | LC | N/A | 500 m | 2005 | MODIS MCD12Q1 [25] |
| | VCF | % | 250 m | 2005 | MODIS MOD44B [26] |

* Annual incoming solar radiation was computed from the observed solar radiation time [19].

The GLAS waveforms might be degraded by the atmospheric forward scattering, signal saturation, background noise (low cloud), and slope gradient effects. In addition, GLAS shots over non-forested lands were not of interest. This study, thus, adopted the five screening steps of previous studies [16,17] to remove the invalid GLAS shots based on the GLA14 internal quality flags and the ancillary datasets (LC, VCF, and GDEM: see Table S1). From the full-waveform profile of each valid GLAS shot, we computed the distance between signal beginning (W_{SB}) and ground peak (W_{GP}) points using the Gaussian decomposition approach [31]. This distance theoretically represents the maximum tree height within circular GLAS footprint since the W_{SB} and W_{GP} correspond to the highest point of tree and the ground surface elevation, respectively. Here, we additionally employed a simple physically-based slope correction approach of Lee *et al.* [32], taking into account the topographic condition (slope, θ) and GLAS footprint size (d_{GLAS}). The final metric of GLAS-derived maximum tree heights (H_{GLAS}) over the CONNA was calculated using Equation (1). Distribution of final GLAS height at the 1 km resolution is shown in Figure S2a.

Figure 1. Forested area defined by the MODIS LC (MCD12Q1) and VCF (MOD44B) products. Three aggregated forest types (evergreen, deciduous, and mixed forests) with percent tree cover ($\geq 50\%$) were considered in this study.



$$H_{GLAS} = (W_{SB} - W_{GP}) - \frac{d_{GLAS} \cdot \tan \theta}{2} \quad (1)$$

where, H_{GLAS} refers to the GLAS-derived maximum tree heights, respective W_{SB} and W_{GP} represent the signal beginning and the ground peak of GLAS full-waveform, d_{GLAS} is the GLAS footprint size, and θ corresponds to the slope.

2.2.2. Field-Measured Tree Heights

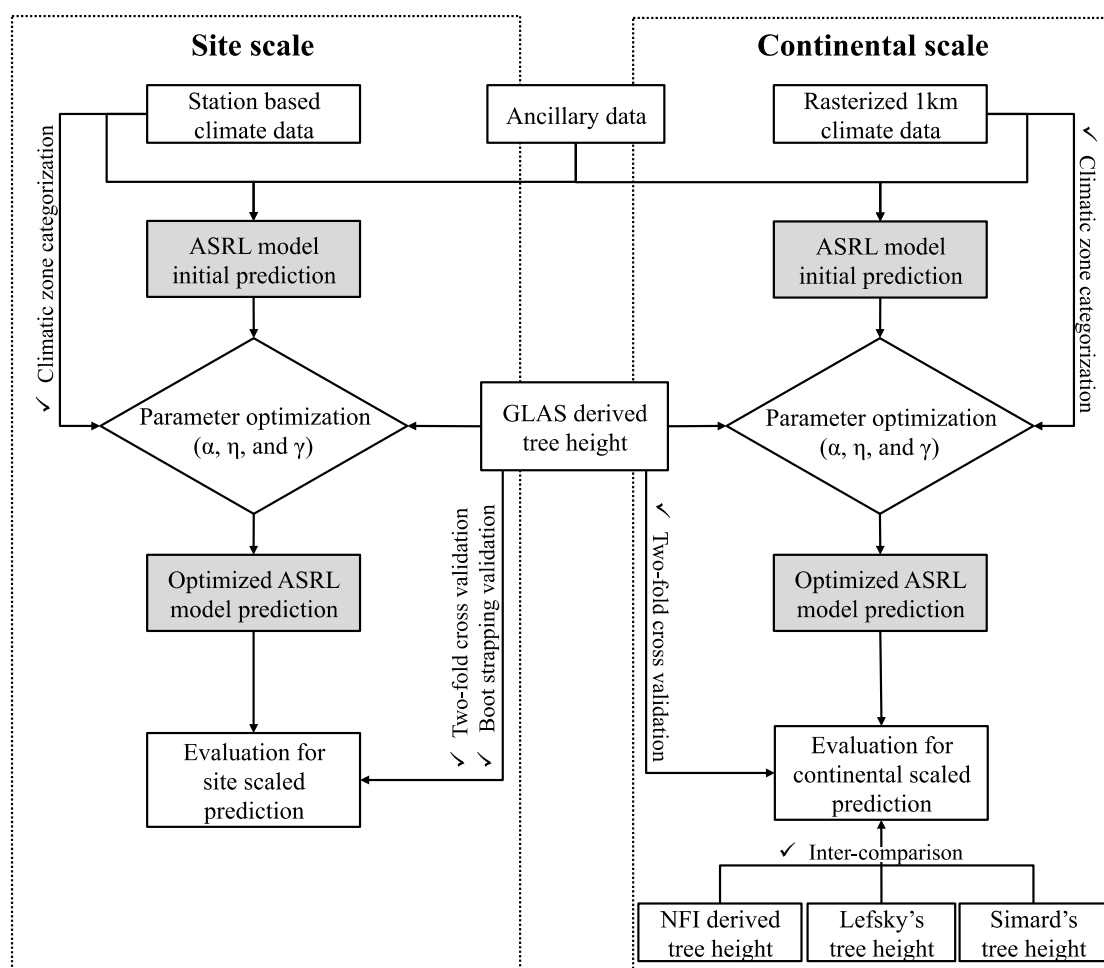
The State Forestry Administration (SFA) of China has systematically investigated national forest resources and updated its database through the repetitive National Forest Inventory (NFI) projects since 1973. In this study, we used tree height information from 5,069,905 plots surveyed for the 7th NFI period (2004–2008) [33]. Most of the NFI sampling plots are squares (25.8 m \times 25.8 m, approximately 0.0667 ha), although some plots have rectangular, round or diamond shapes. Density of plots has been determined by the expected precision level, and distance between plots varies from 2 \times 2 to 8 \times 8 km² [33]. The NFI reports 23 surveyed attributes for each plot (e.g., geo-location, forest type, individual diameter at breast height (DBH), and mean height). To derive maximum tree height (H_{NFI}) for each eco-climate zone, we first developed a power function based allometric equation (Equation (2)) between mean DBH (*i.e.*, averaged individual DBHs) and height information from primary inventory dataset [34–36]. In this process, we extracted and used only 157 effective climate zones with ≥ 20 field surveyed plots (continental scale study). Maximum tree height was then calculated from the largest individual DBH within each effective climate zone under the assumption that the tallest individual tree has the largest DBH. Distribution of *in situ* maximum tree heights is shown in Figure S2b and their locations are limited over the northeastern regions of CONNA. This H_{NFI} will be exploited for model validation only at the continental scale.

$$H_{NFI} = 1.3 + a \cdot DBH^b \tag{2}$$

3. Method

We examined the performance of the optimized ASRL model over the CONNA. Our analysis consisted of two main parts, predicting maximum tree heights at the (a) site and (b) continental scales (Figure 2). This section briefly describes the ASRL model and its optimization process. The model evaluations at both site and continental scales are presented in the following sub-sections.

Figure 2. Overall scheme of research. The performances of the optimized ASRL model was examined over the CONNA. This study was divided into tests at the site and continental scales.



3.1. Overview of the Optimized ASRL Model

The ASRL model can predict the potential maximum tree heights based on a combination of the allometric scaling laws and local resource availability. In this model, hydraulic [13,14] and mechanical [15] constraints determine the potential for tree growth. A key premise of the ASRL is that a tree maintains its evaporative flow by collecting sufficient resources (water and light) while satisfying its basal metabolic needs, in turn, limiting maximum growth. This mechanism can be quantified using a simple inequality ($Q_p \geq Q_e \geq Q_0$) where Q_0 refers to the required metabolic flow rate, Q_e represents the potential

evaporative flow rate, and Q_p corresponds to the available flow rate. These three flows are associated with tree geometry (e.g., canopy radius and leaf area), light (e.g., soil reflectance and leaf absorptivity), and water (e.g., root absorption coefficient and depth of a stomata). The Q_o increases as a tree grows. Simultaneously, the Q_e and Q_p also change but their alterations may occur in different degrees and directions. The ASRL approach, basically, finds a point violating the inequality between given three flow rates. Thus, the intersection either between Q_p and Q_e or between Q_e and Q_o represents a limitation of tree growth, which is the potential maximum height (see [12,16] for more detailed information of the ASRL model).

Although the unoptimized ASRL model might grant a mechanistic understanding in the prediction of potential tree heights [12,16], it still has less predictive power when applied to diverse eco-climatic zones and forest types with varying age classes [16,17]. A plausible reason for this drawback is that the model implements universal allometric coefficients and scaling exponents (e.g., $\alpha = 13 \text{ cm}^2$, $\eta = 1.14$, and $\gamma = 0.33$ as in [12]). Obviously, we expect inconsistent allometric relationships across different environmental conditions. Shi *et al.* [16] recommend a parametric optimization of the ASRL model: such that (a) iteratively adjusts three ASRL parameters (*i.e.*, α , η , and γ) for each eco-climatic zone; and (b) minimizes disparities between the reference and modeled heights, in turn, improving the overall prediction accuracy. Amongst a number of ASRL coefficients and exponents, they have tested those three parameters governing the canopy geometry, energy absorption and transmission, and water absorption capacity of trees [12,16,17]. In this study, we applied the same processes at both site and continental scales. Here, the Powell's optimization approach [37,38] was used for each eco-climatic zone (Section 2.1.3) to enable computationally practical model simulations (see Section S1 and [16] for detail of parametric optimization process).

Powell's optimization algorithm is a straightforward and intuitive optimization process to find the minima of a multidimensional function. This algorithm starts with initial parameter values (e.g., area of single leaf, α , exponent for canopy radius, η , and root absorption efficiency, γ), and the search directions are evaluated sequentially. The best possible improvement in modeled results is explored in a search direction through line minimization methods. Here, it iteratively initializes the parameters before proceeding to the next search direction. In this study, Powell's algorithm minimizes the difference between the reference and modeled tree heights based on a merit function (Press *et al.* [38]; Equation (3)) feasible to optimize three variables.

$$F(p_1, p_2, p_3) = \sum_{k=1}^3 ((p_k - p_{kb})^4 \cdot w_k^2 + \frac{(p_k - p_{k0})^2}{\Delta_{p_k}^2}) + \sum_{i=1}^N \frac{(H_{ASRL,i} - H_{GLAS,i})^2}{\Delta_H^2} \quad (3)$$

$$p_{kb} = \frac{p_{k_lowerL} + p_{k_upperL}}{2} \quad (3.1)$$

$$w_k = 0, \text{ when } p_k \in [p_{k_lowerL}, p_{k_upperL}], \text{ otherwise, } w_k = 10 \quad (3.2)$$

where, p_k is the ASRL model parameter ($k = 1, 2$, and 3 represent α , η , and γ , respectively), p_{k0} refers to the initial values of each parameter, p_{kb} is the boundary limit of each parameter defined by Equation (3.1), and Δ_{pk} is the standard deviation of each parameter value with respect to its initial values. In this process, we set variable ranges (lower and upper boundaries as in the TRY database [39]) of each parametric tree trait ($1 \text{ cm}^2 \leq \alpha < 100 \text{ cm}^2$, $0.8 \leq \eta < 1.5$, and $0.1 \leq \gamma < 0.8$) and initial value of

each parameter ($\alpha = 13 \text{ cm}^2$, $\eta = 1.14$, and $\gamma = 0.33$ according to Kempes *et al.* [12]). w_k is a scalar weight set by the condition in Equation (3.2), N is the total number of comparison sets (i) for GLAS height (H_{GLAS}) and the model prediction (H_{ASRL}) with given parameter values for each climatic zone and Δ_H is the standard deviation associated with H_{GLAS} and H_{ASRL} . From this iterative process, the minimum of the function $F(p_1, p_2, p_3)$ of each climatic zone was derived to predict maximum tree height.

3.2. Site Scale Model Simulation

Among 754 available meteorological stations (537 eco-climatic zones), this study selected 14 sites (14 eco-climatic zones) for the site-specific model simulations over the CONNA (Table 2; Figure S1). The selected study sites accounted for a sufficient number of valid GLAS shots ($n \geq 20$) whose geo-locations are concurrently registered within 10 km radius circle from each station. These GLAS data are necessary for the iterative optimization (training) and validation (test) purposes. The initial ASRL predictions were made using the weather station-based input climate and ancillary data for each study site. We then used the Powell's optimization process to calculate the least differences between the GLAS-derived and modeled heights, resulting in 14 sets of the three adjusted ASRL parameters.

In this study, the model evaluations at the site scale maintained independence between the training and test sets of the GLAS data using (a) a two-fold cross validation and (b) a bootstrapping technique. First, the two-fold cross validation assessed the model performance by randomly partitioning the GLAS samples into two equal batches (*i.e.*, training and test sets). Respective training and test GLAS tree heights were used for the ASRL model optimizations and evaluations for each study site. Second, the bootstrapping approach provided more iterations ($n = 250$) in the random splitting of the GLAS data. Each iteration optimized and evaluated the ASRL model in the same way, as did the two-fold cross validation. When interpreting the evaluation results, this study implemented three statistical metrics: RMSE, R^2 , and relative errors ($RE = (H_{obs} - H_{pred})/H_{obs}$; where H_{obs} refers to the observed height and H_{pred} represents the predicted height). RE was an important statistic for determining ASRL model performance due to the large variation in tree heights across study sites.

3.3. Continental Scale Model Simulation

In addition to the site scale test, we also examined the optimized ASRL model at the continental scale (1 km resolution) over the forested lands of the CONNA (Figure 1). Candidate forest pixels for this test lie in the effective eco-climatic zones (409 out of 5805 zones over the CONNA; Section 2.1.3) where ≥ 20 valid GLAS shots were geo-registered. The initial ASRL predictions were carried out over the individual candidate pixels by implementing the gridded climate and ancillary data. Unlike the site-scale test, we formulated the model optimizations at the eco-climatic zone level: assigning identical ASRL parameters if the forest pixels were associated with the same eco-climatic zone. The optimization for every pixel is not practical since there are over a million forest pixels. For each eco-climatic zone, the ASRL parameters were iteratively adjusted to minimize the overall differences between tree heights derived from the valid GLAS data and the ASRL model.

Table 2. 14 selected study sites where ≥ 20 valid GLAS shots were geo-registered within a 10 km radius. The site information includes geo-location (latitude (Lat.) and longitude (Lon.)), forest types, and climatic variables (temperature (Tmp.), precipitation (Pre.), incoming solar radiation (Rad.), wind speed (Wnd.) and relative humidity (Reh.)). The optimized parameter sets (area of single leaf (Opt. α), exponent for canopy radius (Opt. η), and root absorption efficiency (Opt. γ)) were also listed.

| Site ID | Lat. | Lon. | Forest Type * | Tmp. (°C) | Pre. (mm) | Reh. (%) | Rad. (W/m ²) | Wnd. (m/s) | No. GLAS | H_{GLAS} | H_{ASRL} | Opt. α | Opt. η | Opt. γ |
|---------|-------|--------|---------------|-----------|-----------|----------|--------------------------|------------|----------|------------|------------|---------------|-------------|---------------|
| 1 | 52.35 | 124.72 | M | -2.20 | 474.56 | 67.14 | 334.99 | 2.80 | 111 | 13.30 | 13.00 | 9.8710 | 1.1396 | 0.3460 |
| 2 | 51.7 | 124.33 | M | -2.36 | 523.59 | 67.61 | 316.73 | 2.11 | 31 | 14.25 | 14.93 | 12.1840 | 1.1398 | 0.3360 |
| 3 | 48.77 | 121.92 | M | -0.15 | 478.93 | 63.61 | 326.31 | 2.76 | 34 | 13.93 | 14.93 | 10.0960 | 1.1391 | 0.4490 |
| 4 | 42.35 | 126.82 | D | 0.80 | 774.94 | 70.29 | 377.90 | 1.79 | 57 | 14.93 | 13.00 | 12.4840 | 1.1400 | 0.3330 |
| 5 | 41.92 | 124.08 | M | 6.96 | 774.71 | 68.11 | 325.05 | 2.28 | 26 | 20.63 | 21.11 | 7.5630 | 1.1400 | 0.4500 |
| 6 | 41.28 | 125.35 | D | 7.13 | 807.93 | 67.11 | 346.31 | 2.05 | 21 | 13.00 | 16.37 | 11.2010 | 1.1399 | 0.3450 |
| 7 | 24.02 | 97.85 | E | 20.64 | 1441.78 | 77.14 | 307.46 | 0.93 | 20 | 25.40 | 27.22 | 9.1110 | 1.1400 | 0.4490 |
| 8 | 22.78 | 100.97 | E | 18.83 | 1487.57 | 77.54 | 308.95 | 0.91 | 22 | 37.62 | 38.50 | 6.3760 | 1.1400 | 0.4490 |
| 9 | 26.33 | 114.5 | M | 18.71 | 1483.12 | 78.68 | 321.19 | 1.90 | 20 | 32.75 | 29.18 | 5.3600 | 1.1399 | 0.5250 |
| 10 | 30.62 | 118.98 | M | 15.75 | 1496.55 | 79.46 | 355.40 | 1.68 | 24 | 31.27 | 32.75 | 6.7490 | 1.1399 | 0.4480 |
| 11 | 27.33 | 117.47 | M | 18.13 | 1845.65 | 80.86 | 318.44 | 0.81 | 25 | 30.56 | 31.27 | 10.7320 | 1.1392 | 0.3440 |
| 12 | 27.05 | 118.32 | M | 18.99 | 1682.30 | 80.82 | 290.53 | 1.22 | 21 | 39.40 | 39.40 | 5.1350 | 1.1398 | 0.4390 |
| 13 | 26.9 | 117.17 | M | 17.35 | 1781.74 | 84.64 | 283.78 | 0.81 | 24 | 32.00 | 29.86 | 10.1920 | 1.1392 | 0.3470 |
| 14 | 25.72 | 118.1 | M | 12.42 | 1712.21 | 87.86 | 345.39 | 7.09 | 27 | 32.00 | 32.75 | 5.0600 | 1.1399 | 0.5610 |
| | | Mean | | 10.79 | 1197.54 | 75.06 | 325.60 | 2.08 | 33.07 | 25.07 | 25.30 | 8.7290 | 1.1397 | 0.4160 |
| | | SD | | 8.79 | 524.66 | 7.59 | 25.22 | 1.59 | 24.37 | 9.74 | 9.50 | 2.6340 | 0.0003 | 0.0740 |

* E (Evergreen forest), D (Deciduous forest), and M (Mixed forest).

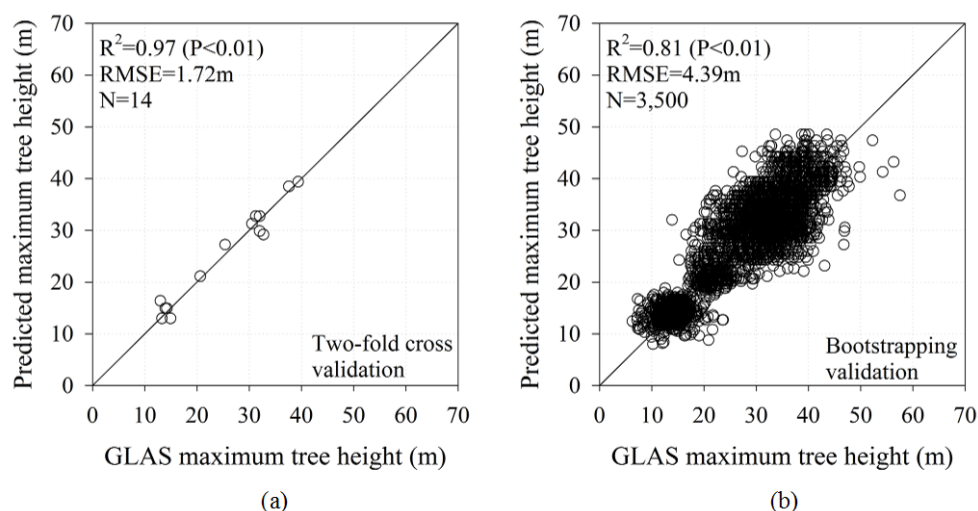
The model evaluations at the continental scale were three-fold: (a) a two-fold cross validation using the valid GLAS altimetry, (b) a comparison to the *in-situ* tree height estimates (H_{NFI} ; Section 2.2.2), and (c) inter-comparison with the existing forest height maps developed by Simard *et al.* [8] (H_{Simard}) and Lefsky [7] (H_{Lefsky}). Just as in the site-scale tests, the two-fold cross validation randomly divided the valid GLAS shots into two equal sets (training and test) for each eco-climatic zone. Additionally, overall means of the modeled tree heights for each eco-climatic zone were assessed by the H_{NFI} . The inter-comparison with H_{Simard} and H_{Lefsky} required pre-processes of the forest height maps, in terms of spatial resolution, projection, and tree height units, to be comparable with our results [16].

4. Result and Discussion

4.1. Predicted Tree Heights at the Site Scale

Following the initial model predictions of the potential maximum tree heights over the 14 selected study sites, three ASRL parameters (α , η , and γ) were iteratively optimized using the independent training GLAS estimates. Results from the two model assessments (two-fold cross validation and bootstrapping) are shown in Figure 3. The optimized ASRL presented a significant agreement between the modeled and test GLAS maximum tree heights ($n = 14$; RMSE = 1.72 m; $R^2 = 0.97$). The performance of the model was satisfactorily stable regardless of the bootstrapping iterations ($n = 14 \times 250 = 3500$; RMSE = 4.39 m; $R^2 = 0.81$). The relative error terms (RE; Figure S3) showed a fairly tight distribution: standard deviation (SD) of RE = 0.09 for the two-fold validation; and SD of RE = 0.17 for the bootstrapping. The optimized ASRL model produced slight overestimations by 2% from the reference tree heights (mean of REs (MREs) = -0.02 in both evaluation cases). These site scale tests over the CONNA are comparable to those over the CONUS documented in Choi *et al.* [17] ($n = 12$; RMSE = 1.81 m; $R^2 = 0.85$; MRE = 0.02 for the two-fold validation, and $n = 500$; RMSE = 2.60 m; $R^2 = 0.66$; MRE = -0.04 for the bootstrapping). The performance of the model was generally stable across different forest ecosystems at the site scale, as supported by this and previous studies resulting in relatively high agreement between the modeled and reference tree heights.

Figure 3. Comparisons between the predicted and test GLAS tree heights over the 14 selected study sites: (a) Two-fold cross validation and (b) bootstrapping approach.



The optimized parameter values significantly varied depending on the different eco-climatic conditions (Table 2). Looking at the adjusted parameters resulting from the optimization, the single leaf area (initial $\alpha = 13.0 \text{ cm}^2$) showed conspicuous change from the initial value (mean = 8.34 cm^2 ; SD = 2.63) while the root absorption efficiency (initial $\gamma = 0.33$) narrowly ranged from 0.33 to 0.56 (mean = 0.42; SD = 0.07). The exponent for canopy radius (initial $\eta = 1.14$) was expected to remain stable, as it was not likely to depend on the eco-climatic conditions (mean = 1.1397; SD = 0.0003). In the sensitivity analysis of single ASRL parameters, Kempes *et al.* [12] also reported stability in η . The morphological characteristics of leaves for each forest type were well represented by α (mean α values for deciduous, evergreen, and mixed forests = 11.84, 7.74, and 8.29 cm^2 , respectively). Interestingly, the γ for evergreen forests (mean $\gamma = 0.45$) showed relatively higher optimized γ values when compared to deciduous forests (mean $\gamma = 0.34$). Similar results for γ have been observed in previous field (e.g., [40,41]), and modeling studies (e.g., [16]). This parametric optimization allows the ASRL model to adjust estimates of canopy geometry, energy absorption/transmission, and hydrological absorption capacity for each study site. The optimized ASRL model successfully represents the balances in evaporative and available flow rates along with the required metabolic flow. This provides a more mechanistic understanding of the relationship between maximum tree heights and concurrent local resource limitations.

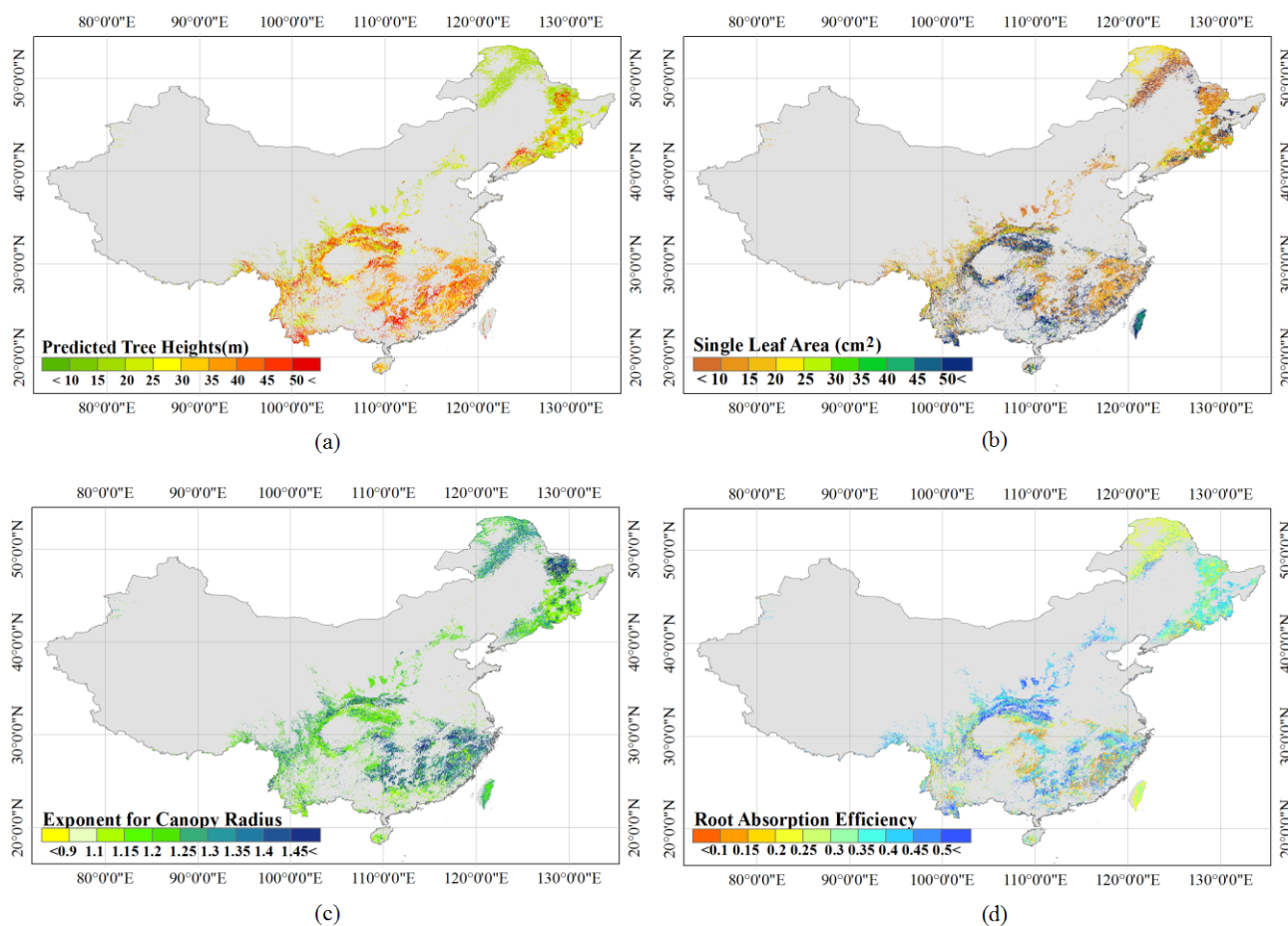
4.2. Predicted Tree Heights at the Continental Scale

A contiguous map of the maximum tree heights over the CONNA (1 km resolution) was generated from the optimized ASRL model using the gridded climate and ancillary data (Figure 4a). This map closely represents the spatial distribution of tree heights in Chinese forests (mean = 36.44 m; SD = 23.85), showing a high correspondence to the spatial pattern of GLAS tree heights (mean = 30.00 m, SD = 6.55; Figure S2a). The optimized ASRL model simulated relatively short tree heights over the northeastern CONNA (Heilongjiang and Inner Mongolia), whereas relatively tall trees were mostly distributed around the central and southern regions (Sichuan, Yunnan, and Chongqing). Such distinct spatial patterns of tree heights were strongly governed by local resource limitations based on water availability and energy balances. Because of sufficiently warm and humid conditions along with high solar energy availability, trees over the southern CONNA likely have higher photosynthetic activity than those under resource-limited conditions (northeastern regions) [42,43]. Some regions including Jilin and Liaoning provinces close to the border of North Korea were likely to show taller tree heights than forests near the border of Russia (Heilongjiang and Inner Mongolia) due to the higher temperature and adequate precipitation in Jilin and Liaoning.

Variations across eco-climatic conditions of optimized ASRL parameters at the continental scale were similar to those at the site scale (Figure 4b–d and Table 2). The α values of each eco-climatic zone were noticeably adjusted to demonstrate the characteristics of tree growth given local resource conditions (Figure 4b). The forest types were satisfactorily reflected in the optimized α (mean α of deciduous, evergreen, and mixed forests = 21.31, 13.96 and 17.51 cm^2 , respectively). Both η (mean = 1.28; SD = 0.19; Figure 4c) and γ (mean = 0.37; SD = 0.15; Figure 4d) did not significantly deviate from the initial values (initial η and $\gamma = 1.14$ and 0.33, respectively), while η and γ still produced distinct spatial distributions across different eco-climatic conditions (described in Section 4.1). We believe that this

spatial pattern of the modeled tree heights represent a degree of predictive power over the CONNA, and the distributions of the optimized parameters support a mechanistic understanding for relationships between the predicted maximum tree height and local resource limitations.

Figure 4. (a) Spatial distribution of tree heights predicted by the optimized ASRL model over the CONNA (1 km resolution). Spatial patterns of the optimized (b) single leaf area; (c) exponent for canopy radius; and (d) root absorption efficiency.

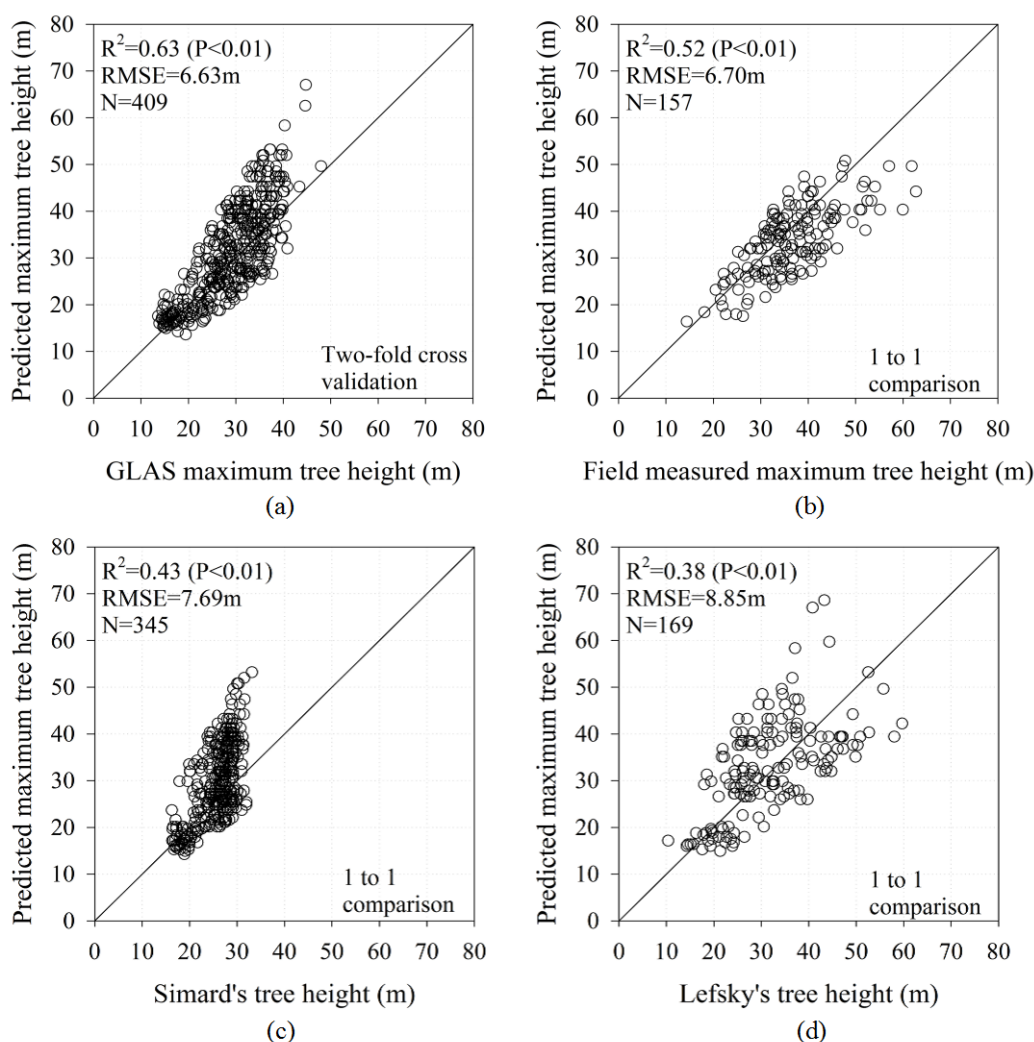


4.2.1. Evaluations Using GLAS and Field Measured Tree Heights

The modeled tree heights at the continental scale were evaluated using (a) the two-fold cross validation with the GLAS altimetry and (b) the one-to-one comparisons with the field-measured tree heights. The two-fold validation showed a moderate agreement between the modeled and independent GLAS data ($n = 409$; $RMSE = 6.63$ m; $R^2 = 0.63$; Figure 5a). The optimized ASRL model predicted 8% taller tree heights than GLAS estimates ($MRE = -0.08$, Figure S4a). This overestimation tended to be distributed over the wet environment (southern CONNA; Figure S5a) where there are likely other competitive factors limiting tree height [12]. Additionally, the available water flow rate (Q_p) may lead to an overestimation of tree heights for the wet forests since the ASRL model neglects soil water behavior and water holding capacity of given soil type and condition. Large underestimations were found in complex terrain regions (high sloped) including Sichuan and Chongqing, and in arid regions near the Gobi desert. Two plausible reasons for the discrepancy over the complex terrain are that

(a) topographic effects on the GLAS altimetry might not be completely rectified by our correction scheme [21,44,45] and (b) input climatic variables are highly sensitive to complex terrain, which might produce large uncertainties [46,47]. The discrepancy over arid regions is likely due to trees that have specialized traits (e.g., drought tolerance) that deviate from the specific parameters used here [12].

Figure 5. Comparisons between the predicted tree height and test GLAS altimetry dataset over the CONNA. (a) Two-fold cross validation between the GLAS height and ASRL model prediction (409 effective climatic zones); (b) comparison between the field-measured height and ASRL model prediction (157 effective climatic zones); (c,d) inter-comparisons between the ASRL predictions and Simard's and Lefsky's height estimations, respectively.



As shown in Figure 5b, the second evaluation (one-to-one comparison) revealed that the optimized ASRL model could explain 52% of the variance of field-measured tree heights ($n = 157$; RMSE = 6.70 m; $R^2 = 0.52$). Here, we noted that the model predicted 6% shorter tree heights when compared to the field-measured tree heights (MRE = 0.06, Figure S4b). Most underestimates were situated over the densely forested northeastern region of the CONNA (Figure S5b). This was likely caused by errors propagated from the training GLAS dataset. The dense forest canopy (e.g., LAI > 4) or the conical crown shaped trees might result in relatively shorter GLAS-derived tree heights [48–50]. In addition,

the ASRL model neglects the forest age, which may be associated with the underestimates because growth rates of the northeastern mature forests (>50 years) might contrast to those of younger forests (<40 years) over the central and southern region of the CONNA [51].

4.2.2. Inter-Comparisons with Other Existing Forest Height Maps

We additionally conducted inter-comparisons with two independent forest height maps. A moderate degree of agreement (RMSE = 7.69 m; $R^2 = 0.43$) was obtained from the comparison between H_{ASRL} and H_{Simard} (Figure 5c), but systematic discrepancies existed between the two tree heights. Simard *et al.* [11] used a different definition of forested lands, which included mosaic crops, open forest, and saline flooded forests. Also, their regression model of tree heights did not allow the prediction of forest heights > 40 m. Thus, the predicted tall trees (>40 m) over the CONNA produced larger errors when compared to H_{Simard} . Inter-comparison with H_{Lefsky} (Figure 5d) implemented Lefsky's input GLAS-based tree heights, rather than the Lorey's height as in [7]. As depicted in Figure 5d, the optimized ASRL model explained approximately 40% of the variance ($R^2 = 0.38$) of H_{Lefsky} . However, this comparison showed larger differences between the modeled tree heights and H_{Lefsky} (RMSE = 8.85 m). These relatively large errors might be caused by the difference in GLAS height retrieval processes between this study (standard Gaussian decomposition) and Lefsky's study (statistical approach).

4.3. Limitations and Further Directions

The evaluation procedures at both scales showed that the optimized ASRL model has the potential to be applied to different forest ecosystems. We successfully demonstrated the spatio-temporal variability of tree heights over the CONNA across various eco-climatic zones and forest types. Nevertheless, the optimized ASRL model still produced larger uncertainties (Figures 3 and 5). These uncertainties might be explained by considering limitations from external (a,b) and internal (c,d) factors: (a) quality of input climate and GLAS data; (b) consistency of sampling scheme; (c) consideration of forest age and soil condition; and (d) selection of optimized scaling parameters.

Climate variables (e.g., precipitation and wind speed) are generally highly sensitive to topography and land cover conditions due to radiative and hydrological properties [52,53]. Thus, the quality of climate variables varies depending on the interpolation methods [54,55]. Since climatic variables largely determine resource conditions errors may be induced when resources, quantified by climate variables limit height growth rates. In addition, the topographic correction of GLAS data may still produce errors due to the simplified footprint size/shape and the simple slope correction scheme [17,44]. It is well known that due the radiative characteristics of lidar waveform, the tree height retrievals are strongly influenced by the asymmetric shapes and sizes of an individual footprint, off-nadir angles, sensor zenith/azimuth angle, and slope orientation conditions [48,56]. The uncertainty induced from the GLAS height retrieval might propagate and influence the final ASRL height product. Input data quality is an ongoing challenge, and these issues should be resolved through further related studies [48,54–56].

In the case of the sampling scheme, this study assumed that the number of valid GLAS shots (≥ 20 footprints) and field plots (≥ 20 plots) were sufficient to reflect the variability of local tree heights for each climate zone. In practice, however, our assumption suffered from the sequential discrete GLAS

footprints along with ascending or descending orbits and roughly gridded field measurements. In other words, sampling scheme limitations and aforementioned uncertainty of GLAS retrieval [21,44,45] collectively caused disagreement between tree height distributions derived from GLAS altimetry, field observation, and the optimized ASRL model (Figure S5). This problem seems ineludible in this study, yet we expect solutions from newly planned field and 3D Earth observing campaigns (e.g., iss-jem Lidar for Observation of Vegetation Environment [57]).

Forest age and soil condition are important drivers in the physical/physiological mechanisms for tree growth. Topographic characteristics and soil texture primarily determine the water availability, which is associated with tree metabolism [58]. Thus, neglecting soil condition may degrade predictive power across diverse eco-climatic regions, because the modeled internal plant flow rate may not fully explain the actual water flow rate. We assumed that GLAS heights bring indirect information about forest age into the ASRL model, however more explicit forest age-based scaling parameters may be needed to improve model performance. To alleviate these influences, subsequent studies will incorporate soil water capacity [58] and stand age [59] maps.

In this study, we optimized three selected ASRL parameters (α , η , and γ) that are strongly associated with the canopy radiation energy budget and precipitation uptake rate of trees. Other parameters (e.g., stomatal density) were optimized by Kempes *et al.* [12], which also showed better prediction than that of the unoptimized ASRL model. As seen in this and previous studies, parametric optimization clearly improves the predictive power of the model. Thus, further study will explore the applicability of optimizing additional other ASRL model parameters.

5. Concluding Remarks

Our multi-article series ultimately aims to produce spatially continuous maps of forest heights and biomass using the Allometric Scaling and Resource Limitation (ASRL) approach. This third study tested the feasibility of the optimized ASRL model over the Continental China (CONNA) at both site (14 study sites) and continental scales. The Geoscience Laser Altimeter System (GLAS) data were used for model optimization. Three selected ASRL parameters (area of single leaf, α ; exponent for canopy radius, η ; and root absorption efficiency, γ) were adjusted to minimize the differences between the reference (GLAS and *in situ* data) and modeled tree heights.

In the site-scale tests, the optimized ASRL model was assessed using the two-fold cross validation and bootstrapping evaluation. Both evaluations maintained the independence between training and test GLAS data. Results of the two-fold cross validation at the 14 study sites showed that predicted tree heights could explain 97% of the variability in reference tree heights (here, GLAS altimetry). On average, estimated height errors were 1.72 m. The model performance was sufficiently stable regardless of bootstrapping iterations ($n = 250$ random splitting of training and test data). This exercise also indicated that the optimized ASRL model produced satisfactory predictive power (RMSE = 4.39 m; $R^2 = 0.81$) at the site scale.

With regard to the continental-scale tests, the GLAS and *in-situ* tree heights were exploited for evaluation purposes. The existing forest height maps (H_{Lefsky} [7] and H_{Simard} [8]) were also used for inter-comparison. The model was capable of showing reasonable correspondence with GLAS and *in-situ* datasets (RMSE = 6.63 m; $R^2 = 0.63$ against the GLAS, RMSE = 6.70 m; $R^2 = 0.52$ against

in-situ). The predicted heights tended to be overestimated (8%) and underestimated (6%) when comparing to the GLAS and *in-situ* tree heights, respectively. The inter-comparison indicated that the optimized ASRL model generated a moderate degree of agreement to H_{Simard} (RMSE = 7.69 m; $R^2 = 0.43$) and to H_{Lefsky} (RMSE = 8.85 m; $R^2 = 0.38$). The modeled tree heights were overestimated when compared to H_{Simard} while being underestimated when compared to H_{Lefsky} —these discrepancies might be influenced by the different definitions of the tree height and forested land among these studies.

We have assessed the feasibility of the model to different forest ecosystems (Chinese forests). The optimized ASRL model satisfactorily performed across scales (both site and continental scales), and has also provided a mechanistic understanding of relationships between tree heights and local resource limitations. Unlike previous works, this study made attempts to evaluate the model using *in situ* maximum tree heights. In this multi-article series, subsequent studies for tree height prediction will also test the optimized ASRL model over different study sites (e.g., Amazonian Basin) in addition to the CONNA. After addressing the discussed limitations, we are interested in the woody biomass prediction using the same methods as in this series. To examine the feasibility of using the model for biomass prediction, further study will begin by assessing performance of the model at the site and continental scales of the continental US.

Acknowledgment

The authors would like to thank Joshua Mantooth for his helpful review of this paper. Thanks also to the three anonymous reviewers whose comments significantly improved this manuscript. This study was partially funded by the National high Technology Research and Development Program of China (863 Program) (Grand No. 2013AA12A302). This work was also supported by the Fulbright Program for graduate studies and NASA Headquarters under the NASA Earth and Space Science Fellowship Program—Grant “NNX13AP55H”.

Author Contributions

The analysis was performed by Xiliang Ni, Taejin Park, Sungho Choi and Yuli Shi. All authors contributed with ideas, writing and discussions.

Conflicts of Interest

The authors declare no conflict of interest.

Reference

1. Chambers, J.Q.; Asner, G.P.; Morton, D.C.; Anderson, L.O.; Saatchi, S.S.; Espírito-Santo, F.D.; Palace, M.; Souza, C. Regional ecosystem structure and function: Ecological insights from remote sensing of tropical forests. *Trends Ecol. Evol.* **2007**, *22*, 414–423.
2. Fang, J.; Chen, A.; Peng, C.; Zhao, S.; Ci, L. Changes in forest biomass carbon storage in China between 1949 and 1998. *Science* **2001**, *292*, 2320–2322.
3. Turner, D.P.; Koerper, G.J.; Harmon, M.E.; Lee, J.J. A carbon budget for forests of the conterminous United States. *Ecol. Appl.* **1995**, *5*, 421–436.

4. Myneni, R.; Dong, J.; Tucker, C.; Kaufmann, R.; Kauppi, P.; Liski, J.; Zhou, L.; Alexeyev, V.; Hughes, M. A large carbon sink in the woody biomass of northern forests. *Proc. Natl. Acad. Sci. USA* **2001**, *98*, 14784–14789.
5. Saatchi, S.S.; Harris, N.L.; Brown, S.; Lefsky, M.; Mitchard, E.T.A.; Salas, W.; Zutta, B.R.; Buermann, W.; Lewis, S.L.; Hagen, S.; *et al.* Benchmark map of forest carbon stocks in tropical regions across three continents. *Proc. Natl. Acad. Sci. USA* **2011**, *108*, 9899–9904.
6. Baccini, A.; Goetz, S.; Walker, W.; Laporte, N.; Sun, M.; Sulla-Menashe, D.; Hackler, J.; Beck, P.; Dubayah, R.; Friedl, M. Estimated carbon dioxide emissions from tropical deforestation improved by carbon-density maps. *Nat. Clim. Chang.* **2012**, *2*, 182–185.
7. Lefsky, M.A. A global forest canopy height map from the moderate resolution imaging spectroradiometer and the geoscience laser altimeter system. *Geophys. Res. Lett.* **2010**, *37*, doi:10.1029/2010gl043622.
8. Simard, M.; Pinto, N.; Fisher, J.B.; Baccini, A. Mapping forest canopy height globally with spaceborne lidar. *J. Geophys. Res.-Biogeosci.* **2011**, *116*, doi:10.1029/2011jg001708.
9. Zwally, H.J.; Schutz, B.; Abdalati, W.; Abshire, J.; Bentley, C.; Brenner, A.; Bufton, J.; Dezio, J.; Hancock, D.; Harding, D.; *et al.* ICESat’s laser measurements of polar ice, atmosphere, ocean, and land. *J. Geodyn.* **2002**, *34*, 405–445.
10. Hudak, A.T.; Lefsky, M.A.; Cohen, W.B.; Berterretche, M. Integration of lidar and Landsat ETM+ data for estimating and mapping forest canopy height. *Remote Sens. Environ.* **2002**, *82*, 397–416.
11. Nelson, R.; Ranson, K.; Sun, G.; Kimes, D.; Kharuk, V.; Montesano, P. Estimating Siberian timber volume using MODIS and ICESat/GLAS. *Remote Sens. Environ.* **2009**, *113*, 691–701.
12. Kempes, C.P.; West, G.B.; Crowell, K.; Girvan, M. Predicting maximum tree heights and other traits from allometric scaling and resource limitations. *PLoS One* **2011**, *6*, doi:10.1371/journal.pone.0020551.
13. Ryan, M.G.; Yoder, B.J. Hydraulic limits to tree height and tree growth. *Bioscience* **1997**, *47*, 235–242.
14. Koch, G.W.; Sillett, S.C.; Jennings, G.M.; Davis, S.D. The limits to tree height. *Nature* **2004**, *428*, 851–854.
15. Niklas, K.J. Maximum plant height and the biophysical factors that limit it. *Tree Physiol.* **2007**, *27*, 433–440.
16. Shi, Y.; Choi, S.; Ni, X.; Ganguly, S.; Zhang, G.; Duong, H.V.; Lefsky, M.A.; Simard, M.; Saatchi, S.S.; Lee, S. Allometric scaling and resource limitations model of tree heights: Part 1. Model optimization and testing over continental USA. *Remote Sens.* **2013**, *5*, 284–306.
17. Choi, S.; Ni, X.; Shi, Y.; Ganguly, S.; Zhang, G.; Duong, H.V.; Lefsky, M.A.; Simard, M.; Saatchi, S.S.; Lee, S. Allometric scaling and resource limitations model of tree heights: Part 2. Site based testing of the model. *Remote Sens.* **2013**, *5*, 202–223.
18. China Meteorological Data Sharing Service System. Available online: <http://cdc.cma.gov.cn/> (accessed on 15 March 2013).
19. Liao, S.; Jiang, L.; Zhao, H. Estimation of spatial distribution of solar energy resource in China. *Commun. Inf. Sci. Manag. Eng.* **2012**, *2*, 25–28.

20. WorldClim—Global Climate Data. Available online: <http://www.worldclim.org> (accessed on 15 March 2013).
21. Hijmans, R.J.; Cameron, S.E.; Parra, J.L.; Jones, P.G.; Jarvis, A. Very high resolution interpolated climate surfaces for global land areas. *Int. J. Climatol.* **2005**, *25*, 1965–1978.
22. Olea, R.A. *Geostatistics for Engineers and Earth Scientists*; Springer: New York, NY, USA, 1999.
23. Tachikawa, T.; Kaku, M.; Iwasaki, A.; Gesch, D.; Oimoen, M.; Zhang, Z.; Danielson, J.; Krieger, T.; Curtis, B.; Haase, J. ASTER Global Digital Elevation Model Version 2-Summary of Validation Results. Available online: https://lpdaacaster.cr.usgs.gov/GDEM/Summary_GDEM2_validation_report_final.pdf. (accessed on 20 March 2013)
24. Yuan, H.; Dai, Y.J.; Xiao, Z.Q.; Ji, D.Y.; Wei, S.G. Reprocessing the MODIS Leaf Area Index products for land surface and climate modelling. *Remote Sens. Environ.* **2011**, *115*, 1171–1187.
25. Friedl, M.A.; Sulla-Menashe, D.; Tan, B.; Schneider, A.; Ramankutty, N.; Sibley, A.; Huang, X. MODIS Collection 5 global land cover: Algorithm refinements and characterization of new datasets. *Remote Sens. Environ.* **2010**, *114*, 168–182.
26. Hansen, M.C.; DeFries, R.S.; Townshend, J.R.G.; Carroll, M.; Dimiceli, C.; Sohlberg, R.A. Global percent tree cover at a spatial resolution of 500 meters: First results of the MODIS vegetation continuous fields algorithm. *Earth Interact.* **2003**, *7*, 1–10.
27. ESRI (Environmental Systems Research Institute). ArcGIS Desktop 9.2 Help Desk: Resampling Under Data Management. Available online: [http://webhelp.esri.com/arcgisdesktop/9.2/index.cfm?TopicName=resample_\(data_management\)](http://webhelp.esri.com/arcgisdesktop/9.2/index.cfm?TopicName=resample_(data_management)) (accessed on 22 March 2013).
28. Brenner, A.C.; Bentley, C.R.; Csatho, B.M.; Harding, D.J.; Hofton, M.A.; Minster, J.; Roberts, L.; Saba, J.L.; Schutz, R.; Thomas, R.H.; *et al.* *Derivation of Range and Range Distributions from Laser Pulse Waveform Analysis for Surface Elevations, Roughness, Slope, and Vegetation Heights*; Algorithm Theoretical Basis Document Version 4.1; NASA Goddard Space Flight Center: Greenbelt, MD, USA, 2003.
29. Neuenschwander, A.L.; Urban, T.J.; Gutierrez, R.; Schutz, B.E. Characterization of ICESat/GLAS waveforms over terrestrial ecosystems: Implications for vegetation mapping. *J. Geophys. Res.-Biogeosci.* **2008**, *113*, doi:10.1029/2007jg000557.
30. Gong, P.; Li, Z.; Huang, H.; Sun, G.; Wang, L. ICESat GLAS data for urban environment monitoring. *IEEE Trans. Geosci. Remote Sens.* **2011**, *49*, 1158–1172.
31. Hofton, M.A.; Minster, J.B.; Blair, J.B. Decomposition of laser altimeter waveforms. *IEEE Trans. Geosci. Remote Sens.* **2000**, *38*, 1989–1996.
32. Lee, S.; Ni-Meister, W.; Yang, W.Z.; Chen, Q. Physically based vertical vegetation structure retrieval from ICESat data: Validation using LVIS in White Mountain National Forest, New Hampshire, USA. *Remote Sens. Environ.* **2011**, *115*, 2776–2785.
33. Chinese Ministry of Forestry. *Forest Resource Statistics of China (2004–2008)*; Department of Forest Resource and Management, Chinese Ministry of Forestry: Beijing, China, 2009. (In Chinese).
34. Huang, S.; Titus, S.J.; Wiens, D.P. Comparison of nonlinear height-diameter functions for major Alberta tree species. *Can. J. For. Res.* **1992**, *22*, 1297–1304.
35. Fang, Z.; Bailey, R. Height–diameter models for tropical forests on Hainan Island in southern China. *For. Ecol. Manag.* **1998**, *110*, 315–327.

36. Huang, S.; Price, D.; Titus, S.J. Development of ecoregion-based height–diameter models for white spruce in boreal forests. *For. Ecol. Manag.* **2000**, *129*, 125–141.
37. Powell, M.J. An efficient method for finding the minimum of a function of several variables without calculating derivatives. *Comput. J.* **1964**, *7*, 155–162.
38. Press, W.H.; Teukolsky, S.A.; Vetterling, W.T.; Flannery, B.P. Minimization or Maximization of Functions. In *Numerical Recipes in FORTRAN: The Art of Scientific Computing*, 2nd ed.; Cambridge University Press: Cambridge, UK, 1992; pp. 394–445.
39. TRY. Plant Trait Database. Available online: <http://www.try-db.org/TryWeb/Home.php> (accessed on 12 April 2013).
40. Goldstein, G.; Rada, F.; Rundel, P.; Azocar, A.; Orozco, A. Gas-exchange and water relations of evergreen and deciduous tropical savanna trees. *Ann. Sci. For.* **1989**, *46*, S448–S453.
41. Medina, E.; Francisco, M. Photosynthesis and water relations of savanna tree species differing in leaf phenology. *Tree Physiol.* **1994**, *14*, 1367–1381.
42. Nemani, R.R.; Keeling, C.D.; Hashimoto, H.; Jolly, W.M.; Piper, S.C.; Tucker, C.J.; Myneni, R.B.; Running, S.W. Climate-driven increases in global terrestrial net primary production from 1982 to 1999. *Science* **2003**, *300*, 1560–1563.
43. Churkina, G.; Running, S.W. Contrasting climatic controls on the estimated productivity of global terrestrial biomes. *Ecosystems* **1998**, *1*, 206–215.
44. Park, T.; Kennedy, R.; Choi, S.; Wu, J.; Lefsky, M.A.; Myneni, R.B.; Knyazikhin, Y.; Mantooth, J. Application of physically-based slope correction for waveform lidar across different footprint sizes and locations: Tests on airborne and spaceborne lidar. *Remote Sens.* **2014**, under review.
45. Hilbert, C.; Schmullius, C. Influence of surface topography on ICESat/GLAS forest height estimation and waveform shape. *Remote Sens.* **2012**, *4*, 2210–2235.
46. Pandey, G.R.; Cayan, D.R.; Dettinger, M.D.; Georgakakos, K.P. A hybrid orographic plus statistical model for downscaling daily precipitation in northern California. *J. Hydrometeorol.* **2000**, *1*, 491–506.
47. Lundquist, J.D.; Cayan, D.R. Surface temperature patterns in complex terrain: Daily variations and long-term change in the central Sierra Nevada, California. *J. Geophys. Res.-Atmos.* **2007**, *112*, doi:10.1029/2006jd007561.
48. Yang, W.; Ni-Meister, W.; Lee, S. Assessment of the impacts of surface topography, off-NADIR pointing and vegetation structure on vegetation lidar waveforms using an extended geometric optical and radiative transfer model. *Remote Sens. Environ.* **2011**, *115*, 2810–2822.
49. Lefsky, M.A.; Cohen, W.B.; Parker, G.G.; Harding, D.J. Lidar remote sensing for ecosystem studies: Lidar, an emerging remote sensing technology that directly measures the three-dimensional distribution of plant canopies, can accurately estimate vegetation structural attributes and should be of particular interest to forest, landscape, and global ecologists. *BioScience* **2002**, *52*, 19–30.
50. Ni-Meister, W.; Lee, S.; Strahler, A.H.; Woodcock, C.E.; Schaaf, C.; Yao, T.; Ranson, K.J.; Sun, G.; Blair, J.B. Assessing general relationships between aboveground biomass and vegetation structure parameters for improved carbon estimate from lidar remote sensing. *J. Geophys. Res.-Biogeosci.* **2010**, *115*, doi:10.1029/2009JG000936
51. Wang, S.; Chen, J.; Ju, W.; Feng, X.; Chen, M.; Chen, P.; Yu, G. Carbon sinks and sources in China's forests during 1901–2001. *J. Environ. Manag.* **2007**, *85*, 524–537.

52. Dickinson, R.E. Land-atmosphere interaction. *Rev. Geophys.* **1995**, *33*, 917–922.
53. Pielke, R.A.; Avissar, R. Influence of landscape structure on local and regional climate. *Landsc. Ecol.* **1990**, *4*, 133–155.
54. Nalder, I.A.; Wein, R.W. Spatial interpolation of climatic normals: Test of a new method in the Canadian boreal forest. *Agric. For. Meteorol.* **1998**, *92*, 211–225.
55. Apaydin, H.; Sonmez, F.K.; Yildirim, Y.E. Spatial interpolation techniques for climate data in the GAP region in Turkey. *Clim. Res.* **2004**, *28*, 31–40.
56. Pang, Y.; Lefsky, M.; Sun, G.Q.; Ranson, J. Impact of footprint diameter and off-NADIR pointing on the precision of canopy height estimates from spaceborne lidar. *Remote Sens. Environ.* **2011**, *115*, 2798–2809.
57. Asai, K.; Sawada, H.; Sugimoto, N.; Mizutani, K.; Ishii, S.; Nishizawa, T.; Shimoda, H.; Honda, Y.; Kajiwara, K.; Takao, G; *et al.* i-LOVE: ISS-JEM lidar for observation of vegetation environment. *SPIE* **2012**, doi:10.1117/12.981326.
58. Zhou, W.; Liu, G.; Pan, J.; Feng, X. Distribution of available soil water capacity in China. *J. Geogr. Sci.* **2005**, *15*, 3–12.
59. Pan, Y.; Chen, J.M.; Birdsey, R.; McCullough, K.; He, L.; Deng, F. Age structure and disturbance legacy of North American forests. *Biogeosciences* **2011**, *8*, 715–732.

© 2014 by the authors; licensee MDPI, Basel, Switzerland. This article is an open access article distributed under the terms and conditions of the Creative Commons Attribution license (<http://creativecommons.org/licenses/by/3.0/>).